ROZPRAWY INŻYNIERSKIE • ENGINEERING TRANSACTIONS • 34, 1–2, 113–137, 1986
Polska Akademia Nauk • Instytut Podstawowych Problemów Techniki

STRESS ANALYSIS OF BOLTED TENSILE END PLATE CONNECTIONS

J. KWIATKOWSKI, L. A. WINNICKI
and A. KRZYŚPIAK (WARSZAWA)

Experimental and theoretical results are presented concerning the analysis of a steel joint with a prestressing bolt. Theoretical analysis is performed by means of the displacement version of the FEM. Elastic-plastic properties of the material are taken into account, and fictitious contact layers are used to model the friction effects and possible slips between the joint elements. The processes occurring in the joint during stressing and loading differ substantially from those obtained from the standard analysis based upon the simplified model of the joint.

NOTATION

a end plate thickness,
A_s stress area,
$\mathbf{B}$ geometrical matrix,
$d\boldsymbol{\varepsilon}$ increment of total strains vector,
$d\boldsymbol{\varepsilon}^e$ increment of elastic strains vector,
$d\boldsymbol{\varepsilon}^{vp}$ increment of visco-plastic strains vector,
$\mathbf{D}$ material matrix of elasticity,
E Young's modulus,
ε_s increment of the bolt elongation,
F yield condition,
$\mathbf{f}$ nodal force vector,
F_t prestress force,
γ fluidity parameter,
J_2 second deviatoric stress invariant,
$\mathbf{K}_0$ elastic stiffness matrix,
M30 10.9 bolt mark, the first number is one-tenth of the Ultimate Tensile Strength in kgf/mm^2, the second number is the ratio of the yield stress to UTS $\times$ 10
ν Poisson's ratio,
Q plastic potential surface,
$\boldsymbol{\sigma}$ stress vector

σ_i stress intensity,
S_e dimensionless stress intensity,
Δt real/pseudo time step,
$\mathbf{u}$ nodal displacement vector,
Y_0 yield stress,
$Y_{0.2}$ yield stress corresponding to the elongation of 0.2%.

1. Introduction

High-strength bolted connections have lately been used extensively in many countries to be assembled at the building site. Such connections have a number of technical and economical advantages. Their cost compares favorably with that of other forms of bolted connections. They require fewer bolts than the standard bolted joints. One of the technical advantages of these connections is their simplicity. For these reasons it is easier to prepare and use them in assembling on site.

Moreover, such joints eliminate clearances arising under service loading in standard connections and reduce the deformability of structures.

The connections themselves are very stiff and are well sealed to protect them against corrosion. They are also neater in appearance than most types of connections in current use. Such joints can be designed to satisfy the necessary requirements for strength, stiffness and load bearing capacity.

As it is well known, high strength steel bolted connections are divided into two groups: friction grip joints and the end plate joints. In the friction grip joints a service load perpendicular to the bolt axes is transmitted by friction due to clamping force between prestressed steel plates.

Under the tension and bending of the end plate joints the tension load is transmitted mainly by a change of clamping force in the steel plates and by an increase of the tightening force in the bolt. Such joints can perform as friction grip joints as well.

The behaviour of the friction grip joints is relatively simple and it has been investigated both experimentally and analitically.

However, the behaviour of the end plate is fairly complex. Experimental research in this field has lately been conducted mainly for the purpose of determining their load bearing capacity and the required design rules.

Some authors have applied the finite element method to study the behaviour after prestressing of the steel plates.

Cullimore and Eckhart [2] used numerical analysis to study friction grip bolted joints. The bolt which is assumed to produce a uniformly destributed pressure on the outer surface of the plate over an annulus around the bolt hole is replaced by statically equivalent concentrated loads at the

nodes within this annulus. The authors disregarded friction forces between the washer and the plate.

YOSHIMOTO *et al.* [15] applied the finite element technique for finding the pressure distribution in the interface of clamped parts. Their numerical model is, due to symmetry, a quarter of the bolted end plate joint. The numerical results were compared with experimental and theoretical considerations based on the three-dimensional theory of elasticity.

BRELT and COOK [1] introduced the finite element method for the stress analysis of treated bolt-nut connections. The thread zone was replaced by a layer of elements with orthotropic properties. Numerical results for conventional and tapered threads were compared with theoretical and experimental results available in the literature.

SURTEES and IBRAHIM [13] used a linear axisymmetric finite element program to analyse the stress distribution in a bolt head. Circumferential and radial strain distribution at the top surface of the head enabled them to introduce a new method for continuous monitoring of the fluctuating bolt tension. The method is based on the strain measurements mode on the surface of the bolt head.

PANCEWICZ and SZTANDERA [10] worked out the way of deformability determination for friction grip joints on the basis of the finite element method.

The above mentioned analyses were carried out only for prestressing under rather drastic simplifications such as linear elasticity of all materials and no slip between individual parts of the connections.

ROMARO [12] and KWIATKOWSKI *at al.* [6] implemented a simplified model of the tensile end plate connection, assuming a priori a shape of the prestressing zone in the plates. A number of authors have accepted such a simplified model of the end plate joint. The second basic assumption for this model is that, under a certain magnitude of the tensile service load, the initial clamping force in the steel plate dissapears completely and the separation of steel plates follows. The real behaviour of the end plate connection under service load has not as yet been fully explained.

The present authors carried out additional laboratory and numerical experiments on a single end plate joint. The aim of the investigation was to find the strain and the stress distributions in individual members of the joint under prestressing, tensile loading and unloading. Such experiments are difficult and expensive and the data necessary for reliable interpretation of results have often to be taken from locations inaccessible to instrumentation.

In the presence of such difficulties the experimental investigations were accompanied by finite element analysis. Complex elasto-viscoplastic material properties were implemented in the nonlinear approach to stimulate more

realistically the behaviour of the connection including both plastic deformation and slip between particular components of the joint.

In what follows, laboratory experiments are described and the viscoplastic formulation is presented accompanied by the numerical solution.

2. Experimental program and measurement technique

All the investigations were carried out at the Institute for Building Technology in Warsaw, Poland.

Single prestressed bolted end plate connections under tensile loading and unloading were considered as shown in Fig. 1.

The two tubular sections with adequate grips for the Amsler testing machine were connected by means of special annuli with steel plates and the bolt M30 10.9.

Three full scale models were made, the main characteristics of which are shown in Table 1.

The steel grades used and their comparison with American grades are given in Table 2.

Two greater washers under the head and the nut in mode 3 were used to avoid plasticity in the highly stressed zones as well as the yielding near the hole in the steel plate. To get the wires of the strain gauges out

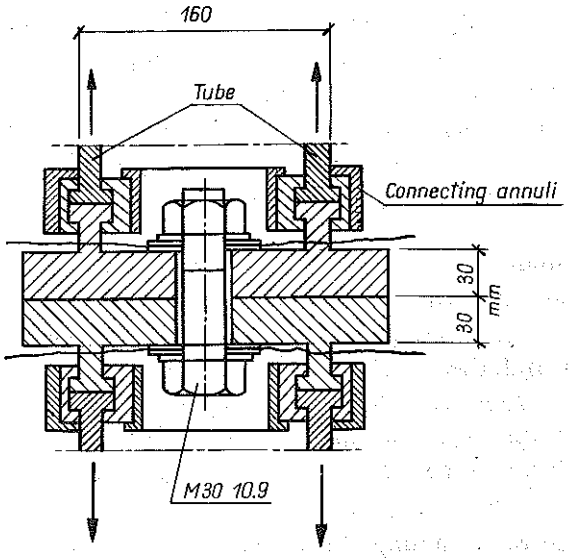

Fig. 1. The main parts of experimental model.

Table 1. Differences between experimental models

Model	Steel plate width 30 mm (1.18 in)	Interface between steel plate cleaned by	Bolt M 30—10.9	Washers quenched and tempered under head and nut pieces
1	Polish Steel St 3S corresponding to ANSI/ASTM A-36	Sandblasting	Bolt diameter 30 mm (1.18 in) conventional thread Steel 50 H corresponding to ANSI/ASTM A 490	1
2		grinding		1
3	Polish Steel 45 corresponding to ANSI/ASTM A 131, AH 36	grinding		2

Table 2. Comparison of Polish and American Steels(*).

	Grades	Yield, point, min, MPa (psi)	Tensile strength, MPa (psi)
Polish	Standard quality carbon Structural Steel for general purposes St 3S	215 ÷ 235 (31200 ÷ 34100)	375 ÷ 460 (54400 ÷ 66700)
American	ANSI/ASTM A 36 Structural steel	250 (36000)	400 ÷ 550 (58000 ÷ 80000)
Polish	High quality carbon Structural Steel for general purposes 45	355 (51500)	600 87000
		280 (40600)	577 (83700)
American	ANSI/ASTM A 131 AH 36, DH 36, EH 36, Structural Steel	350 (50750)	490 ÷ 620 (71100 ÷ 89900)
Polish	Alloyed Structural Steels	Tensile Requirement for Specimens Machined from Bolts	
		Yield Strength (10.2% offset) min	Tensile Strength
	40 H	687 (99600)	932 ÷ 1079 (135100 156400)
	50 H	834 120900	1030 ÷ 1226 (149300 177700)
American	ANSI/ASTM A 490	895 (130000)	1035 ÷ 1170 (150000 ÷ 170000)

(*) According to data available in Poland.

of the models, washers with radial channels were prepared and access holes were drilled through the models, Fig. 1. The hole diameter clearance 7.2 mm greater than the diameter of the bolt shank was provided to protect the gauges against damage. Spiral electrical resistance strain gauges were used along the axis of the bolt and in the plates. The gauges were located in the middle of the length of the bolt shank surface and at different levels of the bolt hole surface in the steel plates, Table 3.

In order to obtain the load-strain relationship, the bolt was suitably calibrated. The bolt was loaded in 5 kN increments up to 80% of the tensile strength and then unloaded with the same steps.

The steel plates were prestressed by means of a pretightened bolt to $F_t = 0.8\, A_s\, Y_{0.2}$ where F_t denotes the prestress force, A_s is the stress area and $Y_{0.2}$ is the yield strength corresponding to the elongation of 0.2%.

The strains were measured and recorded by the automatic gauge system Solatron. Prestressing of the steel plate was carried out in a specially designed device. Service loading and unloading were applied by means of the Amsler testing machine.

3. Theoretical analysis

The behaviour of the laboratory model, Fig. 1, during tightening, loading and unloading indicates that the theoretical analysis must of necessity be complex due to geometrical and physical nonlinearities involved. The numerical model should thus take into account:

possibility of plastic yielding,
varying contact zone and stresses between steel plates,
frictional sliding between components of the connections.

This type of analysis can be classified as physically nonlinear with nonholonomical restrains.

The finite element method has become a very powerful and efficient tool for analysing such complex situations. The elastic finite element solutions satisfying the necessary convergence criteria are now in common use. However, in many situations such a simplified approach fails to describe the real behaviour intensively loaded structures. Although the finite element technique for the linear case is straightforward and unique, the nonlinear solution can be reached in many ways and the results obtained might differ.

For a long time the "initial stress" and the "initial strain" methods have been used for solving plasticity and creep problems. More recently, the visco-plastic approach [16], following Perzyna's formulation [11], has

proved to be an efficient algorithm for problems with material non-linearity.

The basis of visco-plastic formulation, without going into details, is as follows:

The increments of total strains consist of two parts

$$d\boldsymbol{\varepsilon} = d\boldsymbol{\varepsilon}^e + d\boldsymbol{\varepsilon}^{vp}. \tag{3.1}$$

For a stress state $\boldsymbol{\sigma}$ exceeding a certain yield condition

$$F(\boldsymbol{\sigma}, \boldsymbol{\varepsilon}^{vp}) > 0, \tag{3.2}$$

the visco-plastic strain rate $\dot{\boldsymbol{\varepsilon}}^{vp}$ is determined by the constitutive flow rule

$$\dot{\boldsymbol{\varepsilon}}^{vp} = \gamma \langle \phi(F) \rangle \frac{\partial Q}{\partial \boldsymbol{\sigma}}, \tag{3.3}$$

where

$$\langle \phi \rangle = 0 \quad \text{for} \quad F \leqslant 0 \quad \text{and} \quad \langle \phi \rangle = \phi \quad \text{for} \quad F > 0;$$

Q stands for the strain rate potential surface and γ is a fluidity parameter.

The function $\phi(F)$ is chosen either to imitate the real viscous material properties or a simple linear function $\phi(F) = F$ is used which is a distance from a stress point to the yield surface. The linear function is used successfully for solving plasticity problems and this approach is called the pseudo-visco-plastic formulation [16]. The fluidity parameter has no physical meaning — an arbitrary positive value can be taken.

4. Numerical solution

Starting from the standard finite element equilibrium conditions at the element level

$$\int \mathbf{B}^T \boldsymbol{\sigma}\, dv + \mathbf{f} = \mathbf{0}, \tag{4.1}$$

and employing the visco-plastic constitutive law,

$$\boldsymbol{\sigma} = \mathbf{D}(\boldsymbol{\varepsilon} - \boldsymbol{\varepsilon}^{vp}), \tag{4.2}$$

we obtain

$$\int \mathbf{B}^T \mathbf{D}(\boldsymbol{\varepsilon} - \boldsymbol{\varepsilon}^{vp})\, dv + \mathbf{f} = \mathbf{K}_0 \mathbf{u} + \mathbf{f} - \int \mathbf{B}^T \mathbf{D}\boldsymbol{\varepsilon}^{vp}\, dv = \mathbf{0}, \tag{4.3}$$

where $\mathbf{u}$ and $\mathbf{f}$ are the nodal displacement and force vectors, respectively, and $\mathbf{K}_0$ is an elastic stiffness matrix. Therefore, the nonlinear equation (4.1) is substituted by Eq. (4.3) in which the nonlinearity is represented by the

integral treated as an initial load vector. The explicit Euler time stepping procedure was applied to determine this vector in which the values of the n-th time step are used in evaluating the rate of visco-plastic strains for the $(n+1)$-th time step, namely,

$$\boldsymbol{\varepsilon}^{vp} = \boldsymbol{\varepsilon}^{vp} + \Delta t\, \dot{\boldsymbol{\varepsilon}}^{vp}, \tag{4.4}$$

where Δt is a sufficiently small time step in order to ensure the stability of the numerical solution [3].

The system (4.3) is solved for each time step, but as the stiffness matrix $\mathbf{K}_0$ is kept constant, the solution must be executed only once and later on a resolution is required only. This type of solution, if carried out for a sufficient number of time steps to obtain a steady state, will result in an elasto-plastic solution.

As the nature of friction is similar to that of plastic deformation, the pseudo-viscoplastic formulation can be used to satisfy the necessary friction conditions in the bolt' connections. For this purpose we introduce a thin contact layer made of a plastic material obeying a yield surface as in the Coulomb limit friction condition.

For the boundary problem presented here, we assume that the bolts, plates and washers are made of the Huber–Mises type of an elasto-plastic material. The yield function in terms of the second deviatoric stress invariant has the form

$$F = \sqrt{3J_2} - Y_0, \tag{4.5}$$

where Y_0 is the tensile yield stress.

The yield function for the friction modelling contact elements is assumed as the Coulomb limit friction condition, namely

$$F = \tau_{rz} - \sigma_z \tan \varphi, \tag{4.6}$$

where $\tan \varphi$ is a friction coefficient. As steel is known to exhibit plastic incompressibility, the visco-plastic strain rate potential condition can be assumed in the form

$$Q = \sqrt{3J_2}, \tag{4.7}$$

applicable for both materials.

Using the visco-plastic formulation and the above assumption, a FORTRAN finite element computer program has been adopted [7]. The test model shown in Fig. 1 is analysed numerically as an axisymmetric problem and, for simplicity, the double symmetry is assumed. Finite element idealization with 8-node and 6-node contact isoparametric ring elements is shown in Figs. 2 and 3.

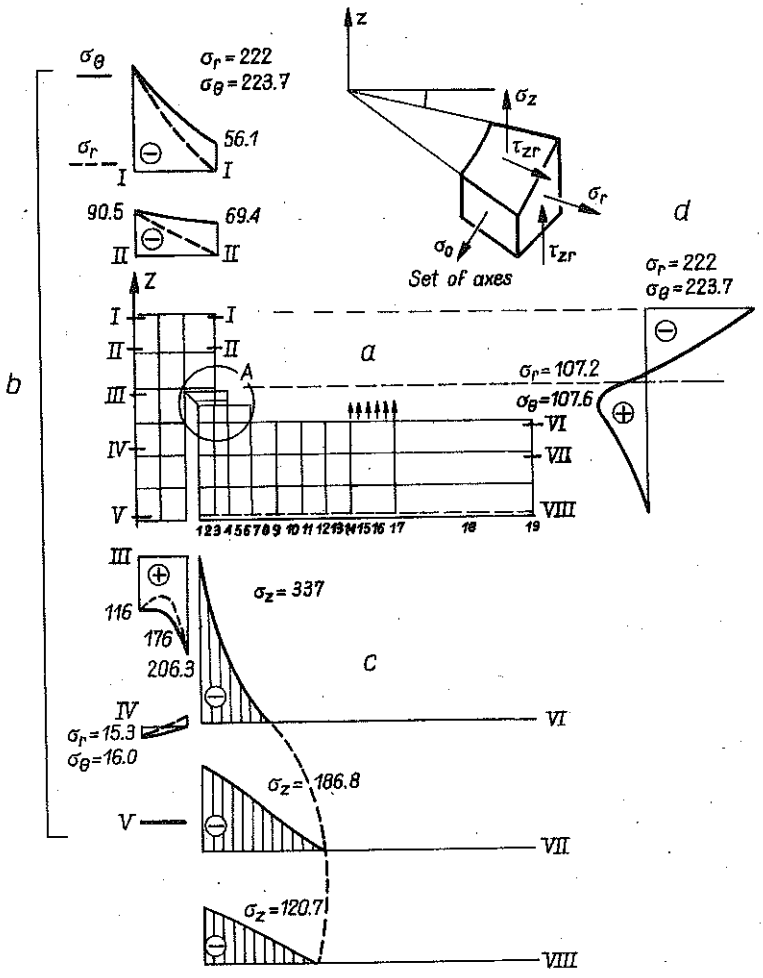

FIG. 2. Finite element stress distribution after initial tightening of the bolt.

For any level of tightening, loading and unloading the deformed profile of the plate element was unknown and had to be determined iteratively. The analysis started with the entire back of the plate supported. When the reactions at any node became tensile, implying that the plate tended to pull away from the support, the node was released and computation was repeated.

Two different types of load were applied. The bolt tightening process was imitated by prescribed displacements applied to the bolt at the plane $z = 0$. The magnitude of this geometrical load was such as to get the recommended pretension force which, in turn, was determined by numerical experiment. The service load was applied to the side of the steel plate

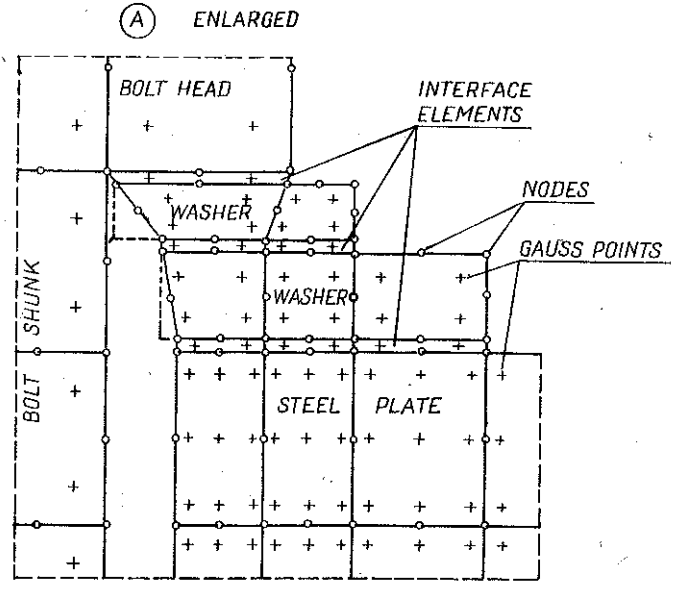

FIG. 3. Part A enlarged, from Fig. 2, of finite element representation of the end plate connection.

as the uniform tension by tube, Figs. 1 and 2. The yield condition was checked in the elemental Gauss points which were densified in the stress concentration zones expected, Figs. 2 and 3.

5. RESULTS AND THEIR ANALYSIS

Only the most significant experimental and numerical results are reported in this paper.

Material data for washers, bolts and steel plates were evaluated from experiments according to Polish Standards. The material properties were found to be as follows:

elastic modulus of bolts and washers $E = 206010$ MPa,
elastic modulus of steel plates $E = 200000$ MPa,
Poisson's ratio $\nu = 0.3$,
friction coefficient $\tan \varphi = 0.32$,
yield strength of bolt and washer $Y_0 = Y_{0.2} = 882.9$ MPa,
yield point of steel plate $Y_0 = Y_{\min} = 352{,}2$ MPa.

The precise definition of a "proof load" appears to vary from country to country. The proof load was assumed here as 90% of the yield load where yield load is taken as the load at a permanent set of 0.2%, see Table 4 for details.

Due to symmetry, one quarter of the end plate connection with two washers was taken into consideration for the finite element discretization, Fig. 2a.

Table 3. Elcctrical resistance strain gauges location.

MODEL No	Number of gauges	
	in the plate hole	On the bolt shunk
1	26	3
2	26	
3	28	

Table 4. Proof load.

Grades	Bolt size mm (in)	Stress Area mm^2 (sq in)	Yield Load or Load at Permanent Set Limit Y_{oz} min kN (lbf)	Tensile Load kN (lbf)	Proof Load kN (lbf)	% of Proof Load / Yield Load
A 490 USA	15.9($\frac{5}{8}$)	146(0.226)	1307(29407)	151(33900)	121(27100)	92.6
	19.05($\frac{3}{4}$)	215(0.334)	192.4(43290)	223(50175)	178 40050	92.5
	31.75($1\frac{1}{4}$)	625(0.969)	559.4(125865)	647(145575)	517(116325)	92.4
A 325 USA						
	3175($1\frac{1}{4}$)	625(0.969)	350(78750)	452(101700)	319 71775	91.1
BS[B] 4395 Port 3 G.B.	16(0.63)	123(0.191)	108.5(24412)	ULTIMATE 120.6(27135)	954(21465)	87.9
	20(0.79)	194(0.301)	171.1(38497)	190.3(42817)	150.5(33862)	88
	30(1.18)	448(0694)	395.1(88898)	439.5 98887	347.6(78210)	88

Table 5. The levels of service loading in numerical solution.

	Elasto-plastic, solution		Elastic solution
	series I	series II	series III
	Force in kN		
	395.6	396.8	Results from series I
Service loading	189.4	—	189.4
	378.7	—	379.7
	410.3	—	410.3
	441.9	—	441.9
	—	456	—
	—	—	473.4
	—	0 (unloading)	—

The numerical solution was carried out for two series of the elasto-plastic model. In comparison with series I, slips in contact layers between connection members were modelled more precisely in series II. Moreover, the solution for service loading being in good agreement with experimental loading immediately after the separation of steel plates, was carried out.

As series III — the elastic solution without contact elements was performed. Table 5 displays all numerical solutions obtained.

The stress diagrams of the results obtained by the numerical solution both in the bolt and the plate for the prestressing are shown in Fig. 2. It should be noticed that the clamping force in the end plate and the tightening force in the bolt are equal to 396.8 KN which is 89.1% of the proof load. In Fig. 2b the diagrams of radial and circumferential stresses in the bolt at various levels are shown. The negative stresses appear to act in the bolt head. Circumferential and radial stress distributions occurring in the bolt axis from the external surface of the bolt head to half of the bolt shank length, are very similar, see Fig. 2d. From the analytical point of view the differences between σ_r and σ_θ stresses should not take place. The differences are due to an extrapolation involving the Gauss points off the bolt axis. The lower central part of the bolt appears to transmit tension, whereas the upper part is under compression. The stresses on the bolt head surface are similar to those obtained by SURTEES and IBRAHIM [13].

Vertical normal stress distribution on three levels as well as the range of the prestressed zone of the end plate are shown in Fig. 2c. The criterion for the boundary of the prestressed zone was taken as that of vanishing σ_z stresses. The maximum negative clamping stresses act near the washers as well as near the bolt hole at all of the load levels of the end plate.

Their distribution under the washer is not linear (level VI) but is almost linear in the contact surface of the steel plates (level VIII) as suggested by PANCEWICZ and SZTANDERA [10].

The σ_z stress and the ε_z strain distributions corresponding to the initial tightening are shown in Fig. 4a. The vertical strain distribution in the bolt at level V is uniform and amounts to 3.4‰. This value corresponds to the bolt tightening force equal to 396.8 kN and is in good agreement with the experimental data. The uniform σ_z bolt stress at level V caused by the forced displacements becomes nonlinear on approaching the bolt head — to level III.

For comparison the ε_z strain distribution in the end plate hole for the finite element model and for the three experimental models are also shown in Fig. 4b. The differences between the experimental results are due to the material properties of the steel plates and due to varying hole diameters and also due to different types of washers. However, for the model 3 the test and numerical results are similar. Moreover, ε_z strain distribution in the end plate hole for a few values of tightening force are presented in

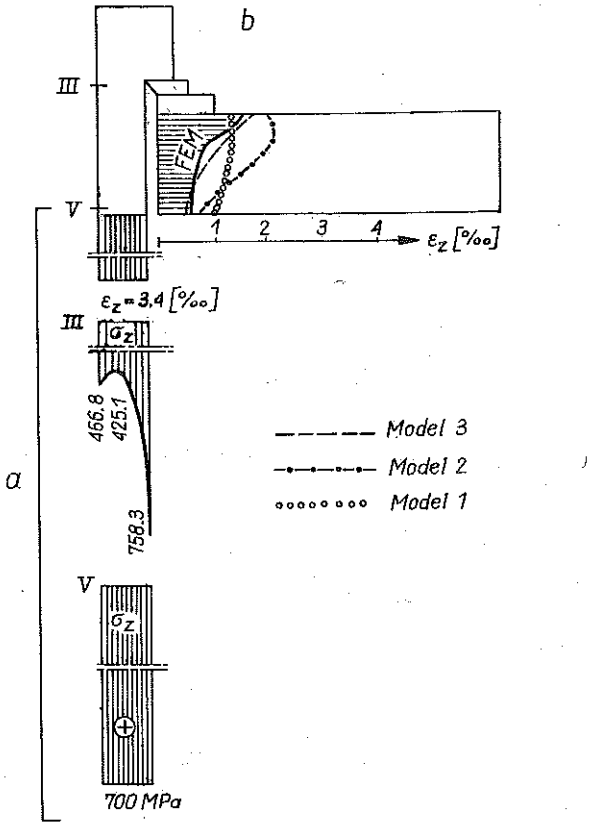

FIG. 4. Stress and strain distribution in the bolt: a) after initial tightening, b) comparison between experimental and numerical results for elasto-plstic solution.

Fig. 5. The finite element results for full clamping force 396.8 kN are also shown.

The ε_z strain distribution in the same place (at the bolt hole) for three levels of the service load are shown in Fig. 6. The comparison between numerical and experimental results shows rather poor agreement here, but the behaviour of these two types is similar. The best agreement exists for the prestressing state. The differences are probably due to some inadequacies in the measurement technique, and also due to difficulties in proper modelling for numerical procedure.

Stresses and strain distribution near the bolt hole at the prestressing state, Fig. 6, is nonlinear as it is assumed in the simplified model. These values decrease on approaching the contact between steel plates. With tension of the prestressed joint the above stresses increase in the first place at

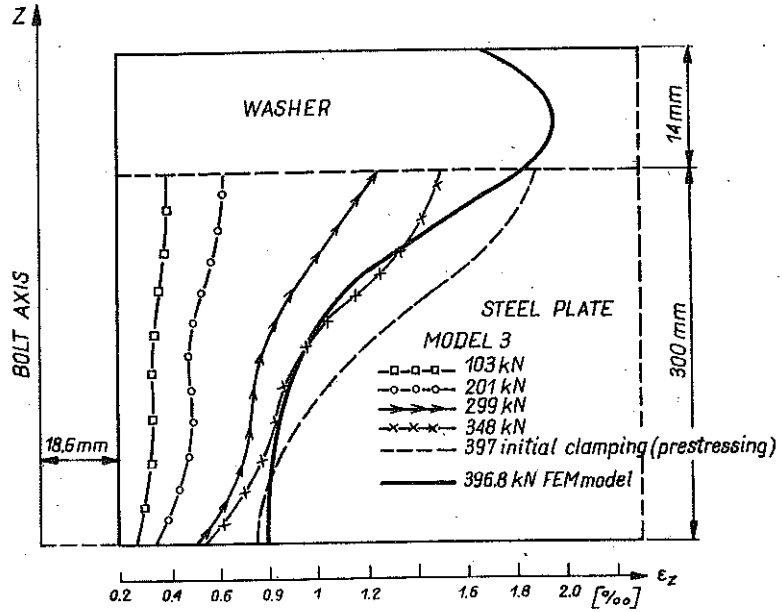

FIG. 5. The vertical strains in the end plate at the bolt hole.

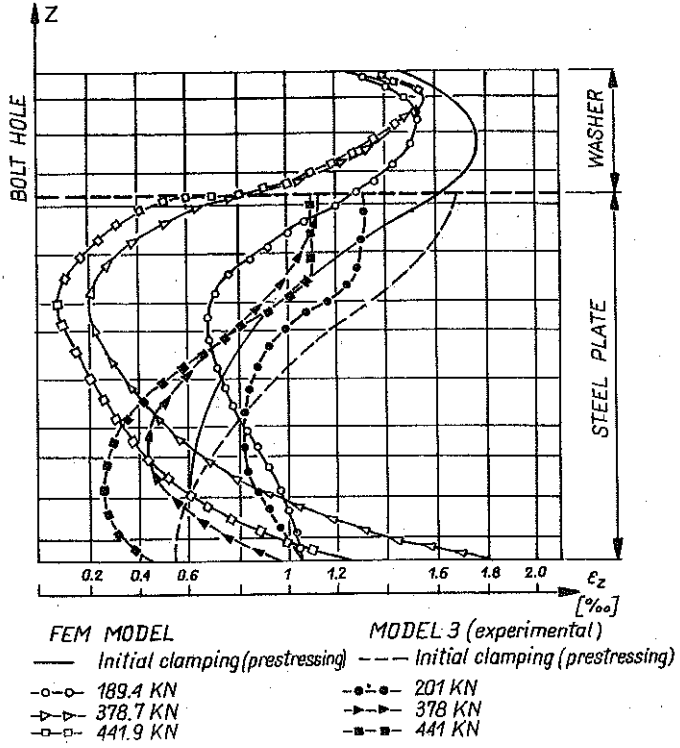

FIG. 6. The vertical strains distributions across of the bolt hole surface. Comparison of the numerical and experimental results.

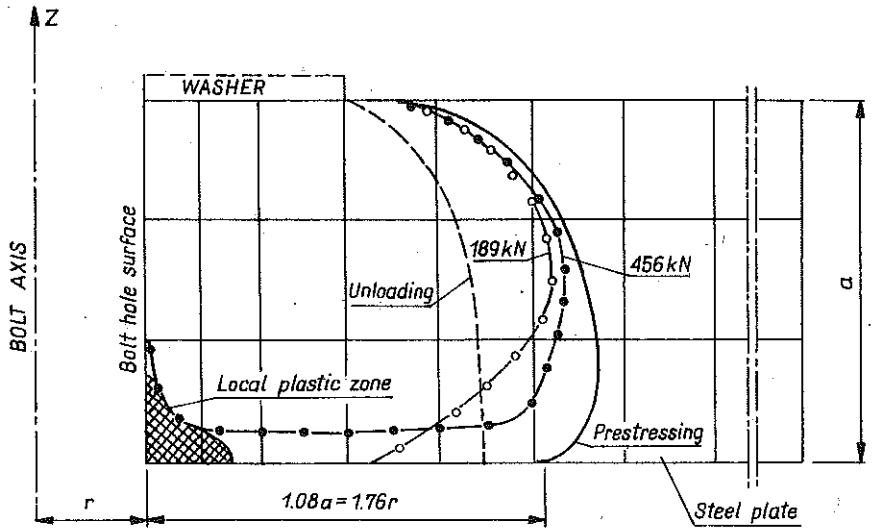

FIG. 7. The range of the clamping zone — finite element elasto-plastic solution.

the interface contact and decrease at the upper part of the plates. With the further increase of tension the stresses decrease.

Figure 7 shows the compressive zone of the end plate for the initial prestressing, for the two levels of service loads and after unloading. The local yielding zone at 456.0 kN which is 102.4% of the proof load is also shown.

In comparison with initial tightening the range of the compressive zone after unloading is decreased. It is the result of the decrease in the tightening force and plastic deformation of the end plate near the bolt hole. It should be noted that the dimension of the compressive zone between the prestressed end plates is about 1.08 of the end plate thickness or 1.76 of the radius of the bolt hole. It is in good agreement with the findings of CULLIMORE and ECKHART [2], PANCEWICZ and SZTANDERA [10] and YOSHIMOTO *et al.* [15].

The service load corresponding to the full separation of the plates is 456.0 kN (102.2% of proof load). Applying this load to the assembly, there is a large compressed area in the steel plates, basically different from that suggested by other authors. It is also different from simplified models by KWIATKOWSKI *et al.* [6] and ROMARO [12]. This phenomenon is related to the flexure of steel plates during the tension of the joint.

Figure 8 shows the isochromes of vertical stresses σ_z in three characteristic states based on the numerical solution in series II. Similar isochromes for radial σ_r and tangential σ_θ stresses were also found. The three-dimensional state of stresses is shown in Fig. 9 by the dimensionless stress intensity

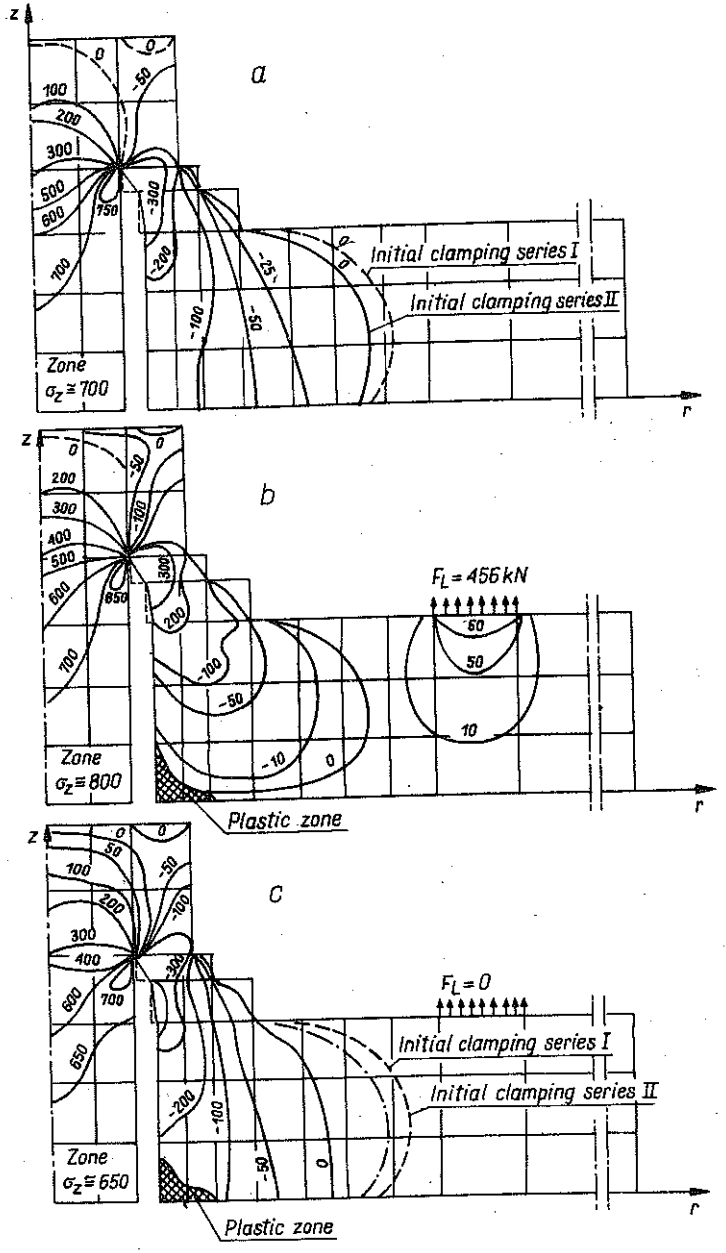

FIG. 8. Isochromes of vertical stress σ_z — elasto-plastic solution; a) after prestressing clamping, b) tensile loading after separation, c) after unloading.

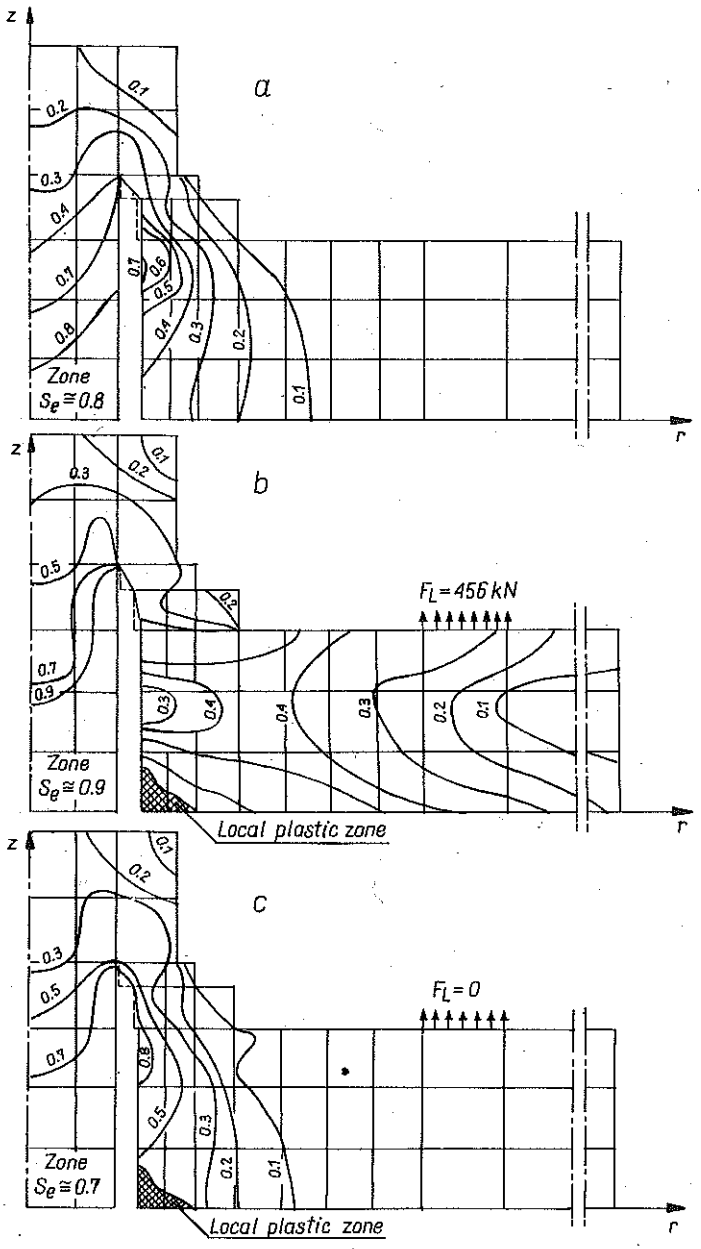

FIG. 9. Isochromes of dimensionless stress intensity S_e — elasto-plastic solution; a) after pre-stressing, b) tensile loading after separation, c) after unloading.

defined as

$$S_e = \frac{\sigma_i}{Y_0},$$

where $S_e = 1$ means the onset of plasticity. The highest S_e exists in the bolt shank and decreases towards the bolt head, similarly to isochromes of vertical stress σ_z. The magnitude of S_e in the bolt shank, corresponding to the tensile force at the instant of separation of the steel plates, see Fig. 9b, increases, according to ROMARO [12] and KWIATKOWSKI [6], by approximately 12%. After unloading, the stress intensity S_e in the bolt and the compression of steel plates decrease approximately by 8%. During tensile loading of the joint the highest S_e exists in the steel plate at the corner of the end plate and near the washers, Fig. 9b.

Partial location of the joint based on numerical solution is shown in Fig. 10a. Dotted line — after initial tightening (magnified 100 times), solid line — after separation of steel plates (magnified 25 times). The changes of steel plate width after pretightening, loading up to separation and unloading of the joint are shown in Fig. 10b. The prestressing is followed by compression (decrease of width) of steel plates — the greatest near the bolt hole. It disappears at the distance of about two lengths of the washer. It corresponds to the compressive zone between the end plates and is in good agreement with the results of other authors. A certain rotation of the end plate outside the contact zone exists there also, Fig. 10a. The washers under the bolt head are subjected to a considerable rotation and the bolt head is displaced and deformed. Under the service load, after separation of steel plates, the decrease of end plate height at the bolt hole, being the result of pretension, is 2.5 times smaller but does not disappear altogether. Under the outer part of the washer and beyond that the thickness of the steel plate is subjected to further decrease, Fig. 10b. Simultaneously, close to the point of application of the service load, the thickness of the end plate increases. The whole end plate rotates around the corner and it is associated with the yielding of this corner. The phenomena described are different from those of the simplified model in which the return to the state before prestressing is assumed. After unloading, the thickness of steel plates returns to the state after initial tightening, Fig. 10b, but near the bolt hole it is slightly decreased due to plastic yielding of the end plate corner.

Diagrams illustrating the correlation between elongation ε_z on the surface of the bolt shank and the tensile service loading after prestressing and during unloading are shown in Fig. 11a. The lines of calibration and experimental results for models 1, 2 and 3 are also given there. These lines start from ε_z bolt strains which correspond to the initial bolt tightening. The points at which those subsequent lines meet calibration lines are denoted by S in Figs. 11a, b. Those points correspond to the separation of steel plates.

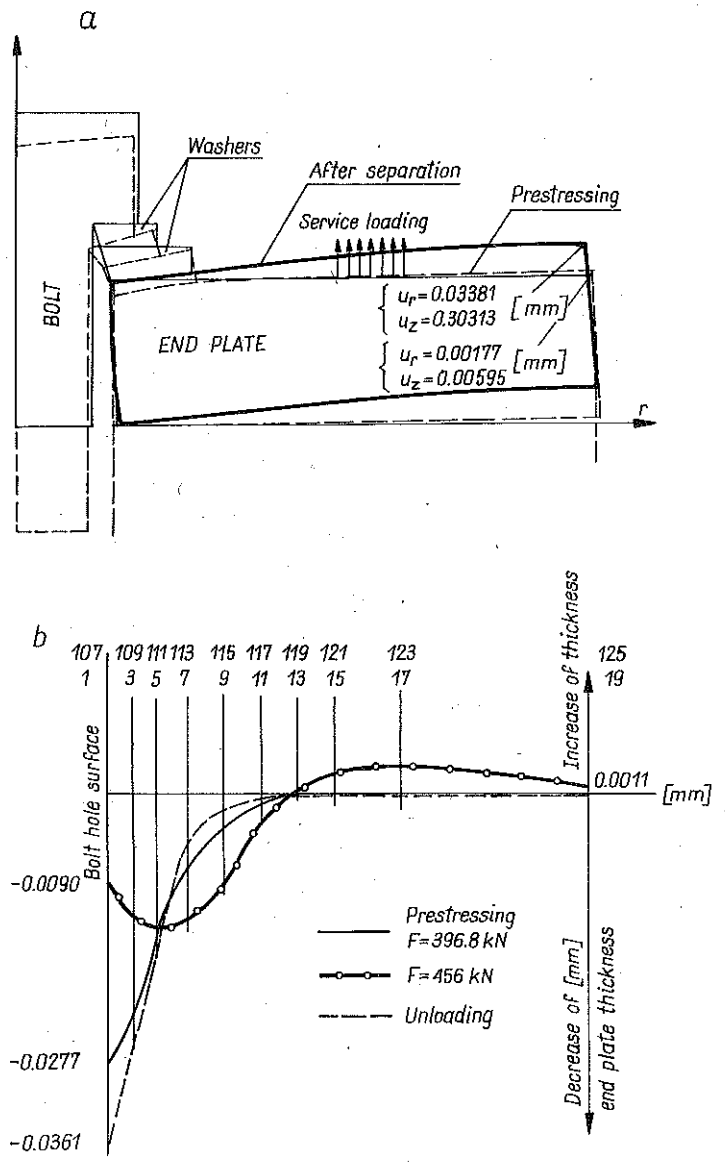

FIG. 10. The state of deformation: a) overall picture, b) variation of end plate thickness along the radius.

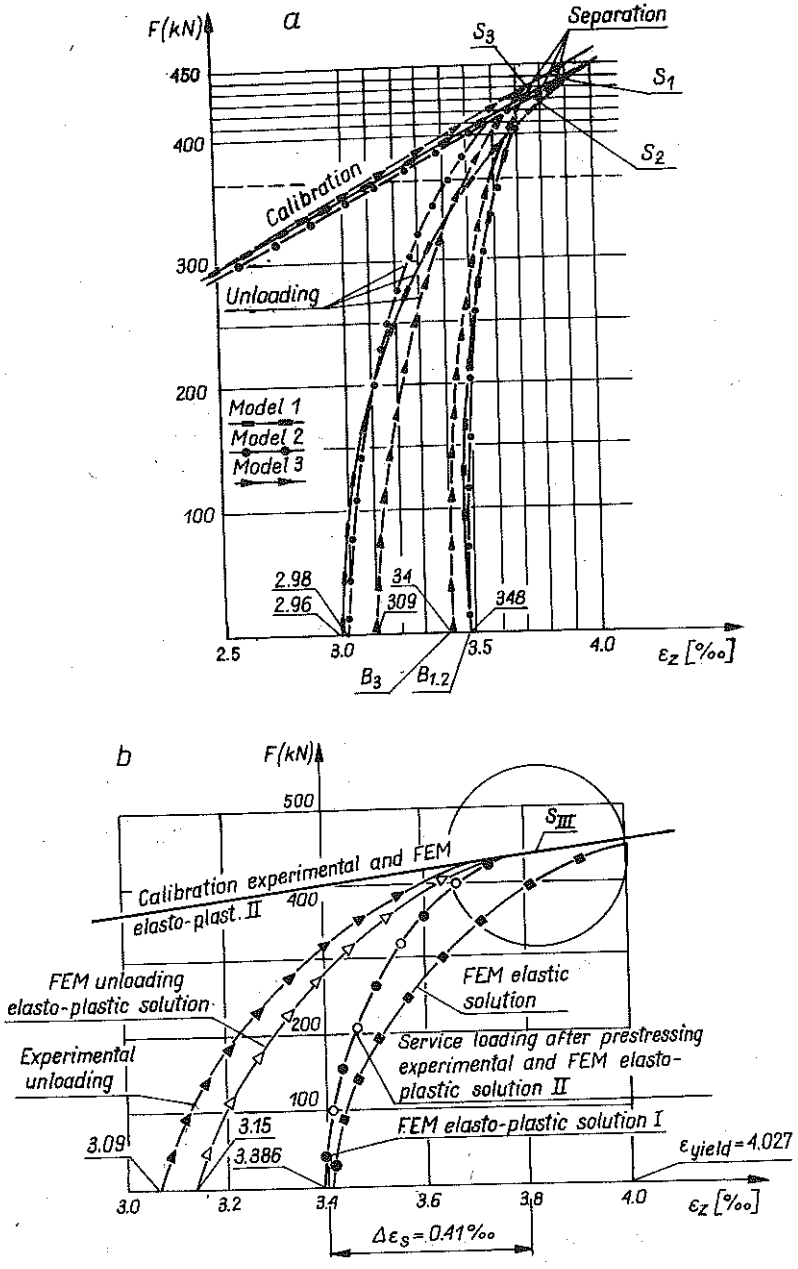

FIG. 11. Correlation between bolt elongation and tensile service loading.

Further loading increase would be transferred by the bolt tension only and the diagram would follow along the line of calibration. The diagrams for model 3 obtained from experiments and numerical solutions are shown in Fig. 11b. The experimental line II and the numerical line in series II are in very good agreement. The numerical results for the elastic solution are found to deviate significantly from the experimental ones.

Diagrams for comparison of phenomena occurring in model 3 according to the simplified model of KWIATKOWSKI *et al.* [6], ROMANO [12] and according to numerical and experimental solution by using adequate lines from the diagrams in Fig. 11b are presented in Fig. 12. The curve $S-L^r$ for numerical elasto-plastic and experimental solutions corresponds with the straight line $S-L^s$ obtained from the simplified model. The separation of the end plate actually takes place at a smaller increase of elementary bolt elongation and with decreased service loading as compared with the simplified model. In fact the role od end plates transmission of service loading is significantly greater than in this model. Moreover the same loading (sections A^s-B^s and A^r-B^r) gives smaller bolt elongation. Figure 12 shows that

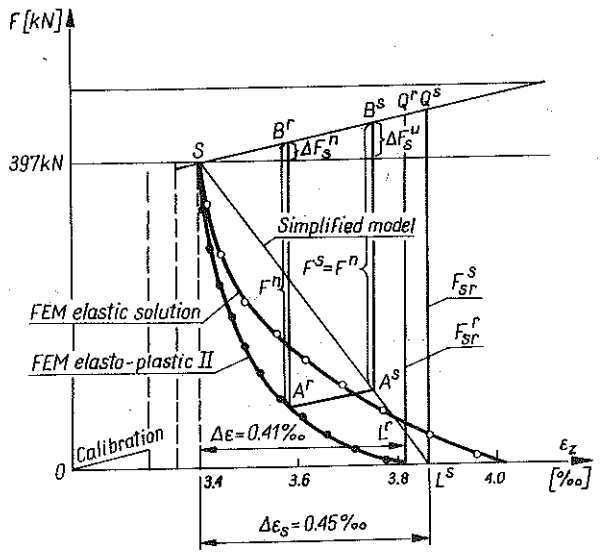

FIG. 12. Behaviour of single bolt end plate connection.

according to the elasto-plastic solution and experimental research, the separation of the end plates takes place at the increment of bolt elongation equal to $\Delta\varepsilon_s = 0.45°/_{oo}$ from the beginning of the initial tightening. This magnitude characterizes at the same time the strain of the whole prestress connection,

Table 6. Significant magnitudes from the investigations of the joint.

	Experimental models			FEM Model 3	
	1	2	3	Elasto-plastic solution I	Elasto-plastic solution II
Initial tightening (force) F_t [kN]	397	397	397	395.6	396.8
ε_z [‰] equal to F_t	3.48	3.48	3.4	3.386	3.4
Service load after separation [kN]	448.5	441.3	446.0	~441	~446
ε_z [‰] equal to separation of end plate	3.95	3.89	3.81	3.80	3.81
Force increment and ε_z in bolt [%]	13.5	11.8	12.1	12.5	12.4
Bolt force after unloading [kN]	337.7	340.0	360.8	—	367.9
ε_z [‰] in bolt after unloading	2.96	2.98	3.09	—	3.15
Ratio of force decrement and ε_z in bolt after unloading to initial tightening [%]	14.9	14.4	9.1	—	7.4

under service loading, Fig. 11. The diagrams show that the same service load applied to conventional, standard connection would cause the bolt elongation equal to 3.81‰, i.e. almost ten times greater than in the prestressed one. The characteristic values resulting from diagrams in Figs. 11a and b are presented in Table 6.

6. Conclusions

The main conclusions based on the analysis of results from experimental as well as numerical or theoretical investigations and concerned with tensile one-bolt end plate connections are as follows:

1. Most of the obtained results for the elasto-plastic finite element solution and the experimental results are found to be in a fairly good agreement, namely:

the vertical ε_z strains on the bolt hole and their distribution across the height of the steel plate for the prestressing, Figs. 4b and 5,

the correlation between elongation of the bolt and the tensile force acting on the joint, Fig. 11,

the total strain of the connection due to service loading, Fig. 11.

The numerical results for the elastic solution are found not to corroborate the test results, Figs. 11 and 12. A part of the numerical results for the elasto-plastic analysis agrees well with the results obtained by other authors. For instance, the radial and the circumferential stress distributions on the surface of the bolt head for the prestressing, Fig. 2b, are almost identical with those published by SURTEES and IBRAHIM [13]. The range of the clamping zone is found to be in good agreement with CULLIMORE and ECKHART [2], PANCEWICZ and SZTANDERA [10] and YOSHIMOTO *et al.* [15]. The stress distributions between the end plate are nearly triangular Fig. 2c, as reported by CULLIMORE and ECKHART [2], PANCEWICZ and SZTANDERA [10]. The local yielding exists at the bolt hole, Fig. 7, as it was also shown by CULLIMORE and ECKHART [2].

On the basis of the above consideration the conclusion may be drawn that the presented method of elasto-plastic finite element analysis with regard to slip between bolt, washers and plates can be successfully used for the determination of the stresses and strains of a one-bolt joint. The numerical solution is found to be superior to experimental investigations. It appears to be an economical way to present a full picture of stresses, strains and displacements during the stages of prestressing, service loading and unloading. It is impossible to obtain such a full picture in tests.

2. There is a large compressed area and local yielding in the steel plates, Fig. 7, during the tension of the prestressed connection at the instant of separation of the end plates. It is different from the simplified model in which, after separation, compressive stresses cannot exist.

3. At the tensile service loading of the joint the following phenomena can be observed in the bolt:

With the increase of tensile service loading the initial tightening force in the bolt also slowly increase, Fig. 11. It is different from the simplified model, Fig. 12, according to which the increase of the tensile bolt-force should have been linear.

The service loadings is carried mainly by steel plates. The real behaviour of the connection is more advantageous than in the simplified model, Fig. 12. At the instant of separation the bolt force increases by 12.4% in the relation to the initial tightening force, what is in good agreement with LAGUNA and ŚLIWKA [8]. After unloading the initial tightening force decreases by 9—15%. With the successive loading of the joint the load bearing capacity decreases. The eventual greater initial tightening should be taken into consideration.

According to this study, the separation of the end plates takes place for a smaller by 9.8% value of bolt elongation in comparison with the simplified theoretical model. It is disadvantageous, if the separation is regarded as the load bearing capacity of the end plate connection. This significant fact should be taken into account as a design rule. The real, earlier separation is the result of the large residual compressive area in the end plates, see Figs. 7 and 8.

4. The experimental and numerical investigations have confirmed the previously known fact, that there exists a considerable stiffness of the end plate joint. Prestressed bolted connection at the service loading corresponding to the separation of end plates has a deformability 10 times smaller than the similar standard connection.

REFERENCES

1. J. L. BRELT and R. D. COOCK, *Modelling the load transfer in threaded connections by the finite element method*, Int. J. Num. Meth. Engng., **14**, 1359—1377, 1979.
2. M. S. C. CULLIMORE and J. B. ECKHART, *The distribution of the clamping pressure in friction-grip bolted joints*, Structural Eng., **52**, 4, 129—131, 1974.
3. I. C. CORMEAU, *Numerical stability in quasi-static elasto-visco-plasticity*, Int. J. Num. Meth. Engng, **9**, 109—128, 1975.
4. R. DELESQUES, *Le calcul des assemblages boulonnes par platine d'extrémite*, Constructions Métalliques, **9**, 4, 55—66, 1972.
5. N. KRISHNAMURTHY, *Modeling and prediction of steel bolted connection behaviour*, Comp. and Struct., **11**, 75—82, 1980.
6. J. KWIATKOWSKI, Z. PANCEWICZ, J. PATORSKI, *High tensile bolted end-plate connection*, [in Polish], Arch. Inż. Ląd., 2, 201—215, 1977.
7. L. A. WINNICKI, and S. A. ZIELIŃSKI, *Finite element program for elasto-visco-plastic stress analysis*, Warsaw Technical Univeristy, Dept. of Civil Engineering, 1978.
8. L. ŁAGUNA, and W. ŚLIWKA, *Doczołowe połączenia elementów konstrukcji stalowych połączone śrubami o wysokiej wytrzymałości*, Inż. i Budown., 4, 139—144, 1977.
9. F. H. NEEDHAM, *Connections in structural steelwork for buildings*, J. Inst. Struct. Engin., **58A**, 9, 267—277, 1980.
10. Z. PANCEWICZ and A. SZTANDERA, *Określenie podatności w złączu sprężonym śrubą wysokiej wytrzymałości*, II Konferencja A. R. T. Olsztyn, 203—208, 1981.
11. P. PERZYNA, *Fundamental problems in viscoplasticity*, Advances Appl. Mech., 9, 1966.
12. G. ROMARO, *Assemblage de profils avec plaques d'about par boulons á haute résistance*, Acier Stahl Steel, **36**, 7—8, 321—328, 1971.
13. J. O. SURTEES, and M. IBRAHIM, *Bolt tension measurement from head strain data*, J. Struct. Div., ASCE, **106**, ST2, 472—490, Feb. 1980.
14. A. SZTANDERA, *Bearing capacity of high bolted connections* [in Polish], Doctor's Theses, Techn. Warsaw Univ., Poland 1979.
15. L. YOSHIMOTO K. MARUYAMA and K. SAWA, *The force ratio of bolted joints*, Bull. JSME, 141, March 1977.
16. O. C. ZIENKIEWICZ and I. C. CORMEAU, *Visco-plasticity, plasticity and creep in elastic solids — a unified numerical solution approach*, Int. J. Num. Meth. Engng., 8, 821—845, 1974.

STRESZCZENIE

ANALIZA NAPRĘŻEŃ W ROZCIĄGANYM POŁĄCZENIU DOCZOŁOWYM NA ŚRUBĘ SPRĘŻAJĄCĄ

W pracy przedstawiono wyniki badań doświadczalnych oraz teoretycznych, dotyczących pracy stalowego połączenia doczołowego sprężonego śrubą. Teoretyczna analiza została przeprowadzona numerycznie przy zastosowaniu metody elementów skończonych w wersji przemieszczeniowej. Uwzględniono w niej sprężysto-plastyczne własności materiału, wprowadzając zaś fikcyjne warstwy kontaktowe modelowano tarcie i ewentualne poślizgi między częściami połączenia. Analizowane tą drogą procesy zachodzące w połączeniu w czasie jego sprężania oraz obciążenia różnią się bardzo od ich ujęcia w stosowanym powszechnie uproszczonym modelu obliczeniowym.

РЕЗЮМЕ

АНАЛИЗ НАПРЯЖЕНИЙ В РАСТЯГИВАЕМОМ ЛОБОВОМ СОЕДИНЕНИИ НА СЖИМАЮЩИЙ ВИНТ

В работе представлены результаты экспериментальных и теоретических исследований, касающихся работы стального лобового соединения сжимаемого винтом. Теоретический анализ проведен численно, при применении метода конечных элементов в версии в перемещениях. Учтены в нем упруго-пластические свойства материала, вводя же фиктивные контактные слои, моделированы трение и возможные скольжения между частями соединения. Анализированные по этому пути процессы, происходящие в соединении во время его сжатия и нагружения, очень отличаются от подхода к ним в применяемой повсеместно упрощенной расчетной модели.

DEPARTMENT OF CIVIL ENGINEERING
WARSAW UNIVERSITY OF TECHNOLOGY, WARSZAWA

Received April 23, 1985.